

Expectile Regularization for Fast and Accurate Training of Neural Optimal Transport

Nazar Buzun

Skoltech, AIRI

N.BUZUN@SKOLTECH.RU

Maksim Bobrin

Skoltech

MAKSIM.BOBRIN@SKOLTECH.RU

Dmitry V. Dylov

Skoltech, AIRI

D.DYLOV@SKOLTECH.RU

Editor: Under Review for COLT 2024

Abstract

We present a new extension for Neural Optimal Transport (NOT) training procedure, capable of accurately and efficiently estimating optimal transportation plan via specific regularisation on conjugate potentials. The main bottleneck of existing NOT solvers is associated with the procedure of finding a near-exact approximation of the conjugate operator (*i.e.*, the c -transform), which is done either by optimizing over maximin objectives or by the computationally-intensive fine-tuning of the initial approximated prediction. We resolve both issues by proposing a new, theoretically justified loss in the form of expectile regularization that enforces binding conditions on the learning dual potentials. Such a regularization provides the upper bound estimation over the distribution of possible conjugate potentials and makes the learning stable, eliminating the need for additional extensive finetuning. We formally justify the efficiency of our method, called Expectile-Regularised Neural Optimal Transport (ENOT). ENOT outperforms previous state-of-the-art approaches on the Wasserstein-2 benchmark tasks by a large margin (up to a 3-fold improvement in quality and up to a 10-fold improvement in runtime).

Keywords: Optimal transport, Neural optimal transport, Conjugate potentials, Non-convex optimization, Expectile regularization.

1. Introduction

Computational optimal transport (OT) has enriched machine learning (ML) research by offering a new view-angle on the conventional ML tasks through the lens of probability measures (Villani et al. (2009); Ambrosio et al. (2003); Peyré et al. (2019); Santambrogio (2015)). Today, OT is primarily employed either 1) as a differentiable proxy, with the OT distance playing the role of a similarity metric between measures, or 2) as a generative model, defined by the plan of optimal transportation. One notable advantage of using OT in latter setting is that, compared to other generative modelling approaches such as GANs, Normalizing Flows, Diffusion Models, there is no assumption for one of the measures to be defined in closed form (e.g Gaussian or uniform), admitting enormous applications of optimal transportation theory. Both loss objective and generative formulations of OT proved to be successful in a vast range of modern ML areas, including generative modelling Arjovsky et al. (2017); Gulrajani et al. (2017); Korotin et al. (2021); Liu et al. (2019b), Leygonie et al. (2019); Bespalov et al. (2022a,b), reinforcement learning Fickinger et al. (2021); Haldar et al. (2023); Papiannidis and Li (2022); Luo et al. (2023), domain adaptation Xie et al. (2019); Shen et al. (2018), change point detection Shvetsov et al. (2020), barycenter estimation Kroshnin et al. (2021); Buzun

(2023), genomics [Bunne et al. \(2022\)](#). Low dimensional discrete OT problems are usually solved via Sinkhorn algorithm [Cuturi \(2013\)](#), which uses *entropic regularisation*, making whole optimization problem differentiable w.r.t to any parameter and computationally efficient, but may require many iterations to converge to optimal solution, whereas the OT problem for tasks supported on high-dimensional measure spaces are usually intractable, oftentimes solvable only for the distributions which admit a closed-form density formulations. As a result, the need for computationally-efficient OT solvers has become both evident [Peyré et al. \(2019\)](#) and pressing [Montesuma et al. \(2023\)](#).

In this paper, we will be concerned with the complexity, the quality, and the runtime speed of the computational estimation of OT plan between two probability measures α and β supported on domains $\mathcal{X}, \mathcal{Y} \subset \mathbb{R}^d$ with Borel sigma-algebra, where the transportation plan $T : \mathcal{X} \rightarrow \mathcal{Y}$ is deterministic and parametrized as a neural network. The OT problem in *Monge's formulation* (MP) for a cost function $c : \mathcal{X} \times \mathcal{Y} \rightarrow \mathbb{R}$ is stated as:

$$\text{MP}(\alpha, \beta) = \inf_{T: T_{\#}\alpha = \beta} \int_{\mathcal{X}} c(x, T(x)) d\alpha(x), \quad (1)$$

where $\{T : T_{\#}\alpha = \beta\}$ is the set of measure-preserving maps between the two measures, defined by a push forward operator $T_{\#}\alpha(B) = \alpha(T^{-1}(B)) = \beta(B)$ for any Borel subset $B \subset \mathcal{Y}$. The minimizer of the cost above exists if \mathcal{X} is compact, α is *atomless* (i.e. $\forall x : \alpha(\{x\}) = 0$) and the cost function is continuous (ref. [Santambrogio \(2015\)](#) Theorem 1.22 and Theorem 1.33).

However, MP formulation of the OT problem is intractable, since it requires finding the maps T under the coupling constraints (which is non-convex optimisation problem) and is not general enough to provide a way for some mass-splitting solutions ([Peyré et al. \(2019\)](#)). It is possible to generalize equation (1) by making OT problem convex through the constraints relaxation, which is known as *Kantorovich problem* (KP) (ref. [Villani et al. \(2009\)](#)):

$$\text{KP}(\alpha, \beta) = \inf_{\pi \in \Pi[\alpha, \beta]} \int_{\mathcal{X} \times \mathcal{Y}} c(x, y) d\pi(x, y) = \inf_{\pi \in \Pi[\alpha, \beta]} \mathbb{E}_{\pi}[c(x, y)], \quad (2)$$

where $\Pi[\alpha, \beta] = \{\pi \in \mathcal{P}(\mathcal{X} \times \mathcal{Y}), \int_{\mathcal{Y}} d\pi(x, y) = d\alpha(x), \int_{\mathcal{X}} d\pi(x, y) = d\beta(y)\}$ is a set of admissible couplings with respective marginals α, β . As was noted above both MP and KP problems are equivalent in case $\mathcal{X} = \mathcal{Y}$ are compact, the cost function $c(x, y)$ is continuous and α is atomless. Moreover, when at least one of the measures has density (absolutely continuous) and ground cost is given as $c(x, y) = h(x - y)$ with h being strongly convex (e.g, squared Euclidean). Theorem 1.17 ([Santambrogio \(2015\)](#)) provides guarantees on uniqueness of the optimal solution to KP and is given by $\hat{\pi} = (\text{Id}, \hat{T})_{\#}\alpha$, meaning that optimal coupling is concentrated on graph of the optimal Monge map \hat{T} .

Since KP (2) is convex, it admits *dual formulation* (DP), which is constrained concave maximization problem and is derived via Lagrange multipliers (Kantorovich potentials) f and g :

$$\text{DP}(\alpha, \beta) = \sup_{(f, g) \in L_1(\alpha) \times L_1(\beta)} \left[\mathbb{E}_{\alpha}[f(x)] + \mathbb{E}_{\beta}[g(y)] \right] + \inf_{\pi, \gamma > 0} \gamma \mathbb{E}_{\pi}[c(x, y) - f(x) - g(y)], \quad (3)$$

where L_1 is a set of absolutely integrable functions with respect to underlying measures α, β . The exchange between *infimum* and *supremum* is possible by strong duality (*Slater's condition*). If one

decomposes the outer expectation \mathbb{E}_π in the last equation as $\mathbb{E}_{\pi(x)}\mathbb{E}_{\pi(y|x)}$, we can notice that the *supremum* by $f(x)$ should satisfy to the condition:

$$f(x) \leq g^c(x) = \inf_{\pi} \mathbb{E}_{\pi(y|x)}[c(x, y) - g(y)] = \inf_{T: \mathcal{X} \rightarrow \mathcal{Y}} [c(x, T(x)) - g(T(x))], \quad (4)$$

otherwise, the *infimum* by γ would yield the $-\infty$ value. Operation g^c is called *c-conjugate* transformation. If MP=KP, the solution $\pi(y|x)$ is deterministic and one may set $\pi(y|x) = T(x)$. Finally, DP (3) may be reduced to a single potential optimisation task (using inequality (4), ref. Villani et al. (2009) Theorem 5.10):

$$\text{DP}(\alpha, \beta) = \sup_{g \in L_1(\beta)} [\mathbb{E}_\alpha[g^c(x)] + \mathbb{E}_\beta[g(y)]] \quad (5)$$

$$= \sup_{g \in L_1(\beta)} \inf_{T: \mathcal{X} \rightarrow \mathcal{Y}} [\mathbb{E}_\alpha[c(x, T(x))] + \mathbb{E}_\beta[g(y)] - \mathbb{E}_\alpha[g(T(x))]] \quad (6)$$

In practice, during optimization process the upper bound of Kantorovich conjugate function $g^c(x)$ is approximated by a parametric model T_θ :

$$g^c(x) \leq g^T(x) = c(x, T_\theta(x)) - g(T_\theta(x)). \quad (7)$$

This rough estimation often leads to the fact that the sum of potentials g and g^T goes to infinity. A number of approaches were proposed to model T_θ in equation (5) *e.g.*, with the Input Convex Neural Networks (ICNN) (Amos et al. (2016); Makkuva et al. (2020); Taghvaei and Jalali (2019)) or with arbitrary non-convex neural networks (Rout et al. (2021); Korotin et al. (2022)). Most of such approaches make assumption on cost to be squared Euclidean and utilize Brenier theorem (Brenier (1991)), from which optimal map recovers as gradient of convex function $\hat{T} = \nabla g^c(x)$. The main bottleneck of these parametric solvers is their *instability in finding the optimal c-conjugate potential* g^T from equation (7). Recently, Amos (2022a) showed that it is possible to find near exact conjugate approximation by performing fine-tuning in order to achieve closest upper bound in the inequality. However, we strongly believe that solution found by fine-tuning can introduce bias by overfitting on current potential optimization step. Moreover, such procedure requires extensive hyperparameter tuning and will definitely introduce an additional computational overhead.¹

In this work, we propose to mitigate above issues by constraining the solution class of conjugate potentials by a new intuitive type *expectile regression* regularization \mathcal{R}_g . Intuitively, we argue that it is possible to measure proximity of potential g to $(g^T)^c$ without an explicit estimation of the infimum in *c-conjugate* transform (4) and instead optimize following objective:

$$\mathbb{E}_\alpha[g^T(x)] + \mathbb{E}_\beta[g(y)] - \mathbb{E}_{\alpha, \beta}[\mathcal{R}_g(x, y)] \approx \mathbb{E}_\alpha[g^T(x)] + \mathbb{E}_\beta[(g^T)^c(y)] \quad (8)$$

We show that such a natural regularization outperforms the state-of-the-art NOT approaches in all of the tasks of the established benchmark for the computational OT problems (the Wasserstein-2 benchmark Korotin et al. (2021)), with a remarkable 5 to 10-fold acceleration of training compared to previous works and achieving faster convergence on synthetic datasets with desirable properties posed on OT map.

1. This intuition is supported by a direct evaluation in Section 5 below.

2. Related Work

In the essence, the main challenge of finding the optimal Kantorovich potentials in equation (5) lies in alternating computation of the exact c -conjugate operators (4). Recent approaches consider the dual OT problem from the perspective of optimization over the parametrized family of potentials. Namely, parametrizing potential as g_η either as a non-convex Multi-Layer Perceptron (MLP) [Dam et al. \(2019\)](#) or as an Input-Convex Neural Network (ICNN) [Amos et al. \(2016\)](#). Different strategies for finding the solution to the conjugate operator can be investigated under a more general formulation of the following optimization [Makkuva et al. \(2020\)](#); [Amos \(2022a\)](#):

$$\max_{\eta} \left[-\mathbb{E}_{\alpha}[g_{\eta}(\widehat{T}(x))] + \mathbb{E}_{\beta}[g_{\eta}(y)] \right], \quad (9)$$

$$\min_{\theta} \mathbb{E}_{\alpha} \left[\mathcal{L}_{\text{amor}}(T_{\theta}(x), \widehat{T}(x)) \right], \quad (10)$$

with $\widehat{T}(x)$ being the fine-tuned argmin of c -conjugate transform (4) with initial value $T_{\theta}(x)$. Loss objective $\mathcal{L}_{\text{amor}}$ can be one of three types of amortization losses which makes $T_{\theta}(x)$ converge to $\widehat{T}(x)$. This max-min problem is similar to adversarial learning where g_{η} acts as a discriminator and T_{θ} finds a deterministic mapping from the measure α to β . The objective in equation (9) is well-defined under certain assumptions and the optimal parameters can be found by differentiating w.r.t. η , according to the Danskin’s envelope theorem [Danskin \(1966\)](#).

We briefly overview main design choices of the amortized models $T_{\theta}(x)$ in the form of continuous dual solvers and the corresponding amortization objective options for $\mathcal{L}_{\text{amor}}$. We mainly base on categorization proposed by [Amos \(2022a,b\)](#), where the following differentiable amortization loss design choices are highlighted:

A. Objective-based learning: ($\mathcal{L}_{\text{amor}} = \mathcal{L}_{\text{obj}}$) methods utilize local information (4) to establish optimal descent direction for model’s parameters θ . [Dam et al. \(2019\)](#) predicts approximate amortized solution $T_{\theta}(x)$ from equation (7) by minimizing the next expression over mini-batch of samples from α :

$$\mathcal{L}_{\text{obj}}(T_{\theta}(x)) = c(x, T_{\theta}(x)) - g_{\eta}(T_{\theta}(x)). \quad (11)$$

Methods max-min [MM] [Dam et al. \(2019\)](#), max-min batch-wise [MM-B] [Mallasto et al. \(2019\)](#); [Chen et al. \(2019\)](#), max-min + ICNN [MMv1] [Taghvaei and Jalali \(2019\)](#), Max-min + 2 ICNNs [MMv2] [Makkuva et al. \(2020\)](#); [Fan et al. \(2020\)](#), [W2OT-Objective] [Amos \(2022a\)](#) use such objective-based amortization in order to learn optimal prediction. However, objective-based methods are limited by computational costs and predictions made by amortized models can be overestimated, resulting in sub-optimal solution.

B. Regression-based Amortization [Amos \(2022b\)](#) ($\mathcal{L}_{\text{amor}} = \mathcal{L}_{\text{reg}}$) is an instance of regression-based learning, which can be done by fitting model’s prediction $T_{\theta}(x)$ into ground-truth solution $\widehat{T}(x)$, taking Euclidean distance as proximity measure:

$$\mathcal{L}_{\text{reg}}(T_{\theta}(x), \widehat{T}(x)) = \|T_{\theta}(x) - \widehat{T}(x)\|^2 \quad (12)$$

Such choice for learning $T_{\theta}(x)$ is computationally efficient and works best when ground-truth solutions $\widehat{T}(x)$ are provided. However, there are no guarantees for obtaining optimal solution when $\widehat{T}(x)$ is not unique.

C. Cycle-based Amortization ($\mathcal{L}_{\text{amor}} = \mathcal{L}_{\text{cycle}}$) is based on the first order optimality criteria for equation (4), i.e $\nabla_y c(x, y) = \nabla_y g_\eta(y)$. If $c(x, y) = \frac{1}{2}\|x - y\|^2$ then $\nabla_y c(x, y) = x - y$ and one may use the following expression in the loss

$$\min_{\theta} \mathbb{E}_{\alpha} \mathcal{L}_{\text{cycle}}(T_{\theta}(x)) = \min_{\theta} \mathbb{E}_{\alpha} \|x - T_{\theta}(x) - \nabla g_{\eta}(T_{\theta}(x))\|^2. \quad (13)$$

It is called *cycle-consistency* regularization. Method [W2] Korotin et al. (2019) uses this choice and substitutes it from the dual loss (9) to avoid solving max-min problem.

However, those approaches either impose unrealistic constraints on parametric family of potentials (e.g ICNNs) or assume that underlying cost is Euclidean. Another approach mitigates all those constraints by introducing regularization term named *Monge gap* (Uscidda and Cuturi (2023)) and learns optimal T map from Monge formulation directly, without any dependence on conjugate potentials. More explicitly, by finding reference measure μ with $\text{Support}(\alpha) \subset \text{Support}(\mu)$, the following regularizer is introduced which quantifies deviation of T from being optimal transport map:

$$\mathcal{M}_{\mu}^c = \mathbb{E}_{\mu}[c(x, T(x))] - \text{KP}^{\varepsilon}(\mu, T_{\#}\mu) \quad (14)$$

with KP^{ε} being entropy-regularized Kantorovich problem (2). However, despite its elegance, we still need some method to compute KP^{ε} and underlying measure μ should be chosen carefully as it's choice will affect recovered optimal map \hat{T} and the case when $\mu = \alpha$ does not always provide desired results.

3. Background

Bidirectional transport mapping. Optimality in equation (5) is obtained whenever complementary slackness is satisfied, namely: $\forall (x, y) \in \text{Support}(\hat{\pi}) : g^c(x) + g(y) = c(x, y)$. Consider a specific setting when the optimal transport plan $\hat{\pi}(x, y)$ is deterministic and $\text{MP}=\text{KP}$. Let the domains of α, β be equal and compact, i.e. $\mathcal{X} = \mathcal{Y}$, for some strictly convex function h the cost $c(x, y) = h(x - y)$. Denote by h^* the convex conjugate of h , implying that $(\partial h)^{-1} = \nabla h^*$. If α is absolutely continuous then $\hat{\pi}(x, y)$ is unique and concentrated on graph $(x, \hat{T}(x))$. Moreover, one may link it with Kantorovich potential $\hat{f} = (\hat{g})^c$ (solution of DP 5) as follows (Santambrogio (2015) Theorem 1.17):

$$\nabla \hat{f}(x) \in \partial_x c(x, \hat{T}(x)) \quad (15)$$

and particularly for $c(x, y) = h(x - y)$

$$\hat{T}(x) = x - \nabla h^*(\nabla \hat{f}(x)). \quad (16)$$

If the same conditions are met for measure β we can express the inverse mapping $\hat{T}^{-1}(y)$ through the potential \hat{g} :

$$\hat{T}^{-1}(y) = y - \nabla h^*(\nabla \hat{g}(y)). \quad (17)$$

Max-min optimisation in problem (5) by means of parametric models f_{θ} and g_{η} is unstable due to non-convex nature of problem. One way to improve robustness is to simultaneously train bidirectional mappings $\hat{T}(x)$ and $\hat{T}^{-1}(y)$ expressed by formulas (16) and (17), thus yielding self-improving iterative procedure.

Wasserstein-2 (W_2) case. For squared Euclidean cost $c(x, y) = \frac{1}{2}\|x - y\|^2$, one may use ordinary conjugation and replace the vector norms outside the supremum in (5). Let Kantorovich potential $g(y)$ equals $\frac{1}{2}\|y\|^2 - u(y)$, then

$$g^c(x) = \inf_y \left(\frac{1}{2}\|x - y\|^2 - \frac{1}{2}\|y\|^2 + u(y) \right) = \frac{1}{2}\|x\|^2 - u^*(x) \quad (18)$$

and consequently from (5) we derive that

$$\frac{1}{2}W_2(\alpha, \beta) = \frac{1}{2}\mathbb{E}_\alpha\|x\|^2 + \frac{1}{2}\mathbb{E}_\beta\|y\|^2 + \sup_{u \in L_1(\beta)} \left[\mathbb{E}_\alpha[-u^*(x)] + \mathbb{E}_\beta[-u(y)] \right]. \quad (19)$$

By equation (17) the corresponding optimal transport map $\hat{T}(x)$ equals to the gradient of \hat{u}^* (argmaximum from the last formula):

$$\hat{T}(x) = x - \nabla \hat{f}(x) = \nabla \hat{u}^*(x). \quad (20)$$

Expectile regression. The idea behind this approach is to minimize the least asymmetrically weighted squares. It is a popular option for estimating conditional maximum of a distribution through neural networks. Let $f_\theta : \mathbb{R}^d \rightarrow \mathbb{R}$ be some parametric model from $L_2(\mathbb{R}^d)$ space and x, y be dependent random variables in $\mathbb{R}^d \times \mathbb{R}$, where y has finite second moment. By definition (Newey and Powell (1987)), the conditional expectile model is:

$$\min_\theta \mathbb{E} \left[\mathcal{L}_\tau(y - f_\theta(x)) \right] = \min_\theta \mathbb{E} \left[\tau - \mathbb{I}[y \leq f_\theta(x)] \right] (y - f_\theta(x))^2, \quad \tau \geq 0.5. \quad (21)$$

The expectation is taken over the $\{x, y\}$ pairs. The asymmetric loss \mathcal{L}_τ reduces the contribution of those values of y that are smaller than $f_\theta(x)$, while the larger values are weighted more heavily (ref. Figure 1). The expectile model $f_\theta(x)$ is strictly monotonic in parameter τ . And particularly the important property for us is when $\tau \rightarrow 1$ it approximates the conditional (on x) maximum operator over the corresponding values of y (Bellini et al. (2014)). Below we compute c-conjugate transformation using the expectile.

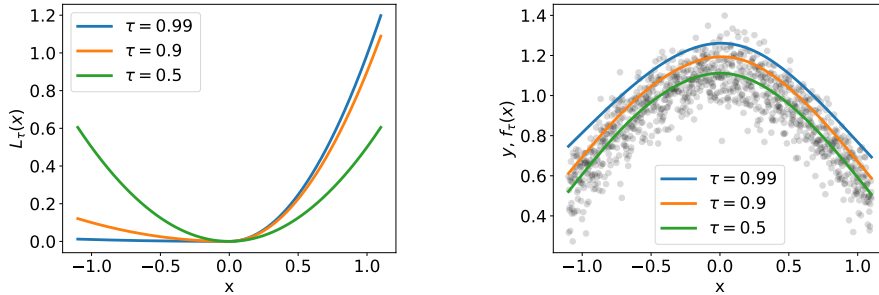


Figure 1: Expectile regression. **Left:** the asymmetric squared loss L_τ . The value $\tau = 0.5$ corresponds to the standard MSE loss, while $\tau = 0.9$ and $\tau = 0.99$ give more weight to the positive differences. **Right:** expectile models $f_\tau(x)$. The value $\tau = 0.5$ corresponds to the conditional statistical mean of the distribution, and when $\tau \rightarrow 1$ it approximates the maximum operator over the corresponding values of y .

4. Proposed Method

The main motivation behind our method is to regularize optimization objective in DP (5) with inaccurate approximation of c -conjugate potential $g^T(x)$, defined in (7). The regularisation term $\mathcal{R}_g(x, y)$ should “pull” $g(y)$ towards $(g^T)^c(y)$ and $g^T(x)$ towards $g^c(x)$. Instead of finding explicit c -conjugate transform, we compute τ -expectile of the distribution governed by functionals of type $g^T(x) - c(x, y)$. From the properties of expectile regression described above and equation (4) follows that when $\tau \rightarrow 1$ the expectile converges to

$$\max_{x \in \mathcal{X}} [g^T(x) - c(x, y)] = -(g^T)^c(y). \quad (22)$$

Denote the parametric models of Kantorovich potentials by $f_\theta(x)$ and $g_\eta(y)$. The transport mapping $T_\theta(x)$ has the same parameters as $f_\theta(x)$ in bidirectional training (ref. 16), or otherwise, when f_θ is not used (one-directional training), it is its own parameters. Combining (21), (22) with (7) we obtain the regularization loss for function g :

$$\mathcal{R}_g(\eta, x, y) = \mathcal{L}_\tau(c(x, T_\theta(x)) - g_\eta(T_\theta(x)) - c(x, y) + g_\eta(y)). \quad (23)$$

Note that in practice, we never set τ very close to 1, since this can cause divergence issues. Proposed expectile regularisation is incorporated into alternating step of learning Kantorovich potentials by implicitly estimating upper bound of distribution over possible c -conjugate potentials, additionally encouraging model g to satisfy the *alternative c -concavity criterion* (Villani et al. (2009) Proposition 5.8). We minimize $R_g(\eta) = \mathbb{E}_{\alpha, \beta} \mathcal{R}_g(\eta, x, y)$ by η and simultaneously do training of the dual OT problem (5) optimising the main objective by θ and η

$$\max_{\eta} \min_{\theta} \mathbb{E}_{\beta} [g_\eta(y)] - \mathbb{E}_{\alpha} [g_\eta(T_\theta(x))] + \mathbb{E}_{\alpha} [c(x, T_\theta(x))], \quad (24)$$

splitting it into two losses

$$L_g(\eta) = -\mathbb{E}_{\beta} [g_\eta(y)] + \mathbb{E}_{\alpha} [g_\eta(T_\theta(x))] \quad (25)$$

and

$$L_f(\theta) = -\mathbb{E}_{\alpha} [g_\eta(T_\theta(x))] + \mathbb{E}_{\alpha} [c(x, T_\theta(x))]. \quad (26)$$

Algorithm 1 describes a complete training loop with joint minimization of $L_g(\eta)$, $R_g(\eta)$ and $L_f(\theta)$ with hyperparameters τ (expectile) and λ (weight of R_g). It includes two training options: one-directional with models g_η and T_θ ; and bidirectional for strictly convex cost functions in form of $h(x - y)$ with models f_θ, g_η and T_θ, T_η^{-1} (the latter are represented in terms of f_θ, g_η by formulas (16), (17)). The bidirectional training procedure updates g_η, T_θ in one optimisation step and then switches to f_θ, T_η^{-1} update in the next step. This option includes analogical regularisation term for the potential f_θ :

$$\mathcal{R}_f(\theta, x, y) = \mathcal{L}_\tau(c(T_\eta^{-1}(y), y) - f_\theta(T_\eta^{-1}(y)) - c(x, y) + f_\theta(x)). \quad (27)$$

In the end of training we approximate the correspondent Wasserstein distance by expression (24) with optimized parameters $\hat{\theta}, \hat{\eta}$.

Algorithm 1 ENOT Training

Input: samples from unknown distributions $x \sim \alpha$ and $y \sim \beta$; cost function $c(x, y)$;
Parameters: parametric potential models f and g , optimizers `opt_f` and `opt_g`, batch size n , train steps N , expectile τ , expectile loss weight λ , bidirectional training flag `is_bidirectional`;

function `train_step`($f, g, \{x_1, \dots, x_n\}, \{y_1, \dots, y_n\}$)

- 1: {Assign OT mapping $T(x)$ }
- 2: **if** `is_bidirectional` is **true** **then**
- 3: {Assume that $c(x, y) = h(x - y)$ **and** h has convex conjugate h^* }
- 4: $T(x) = x - \nabla h^*(\nabla f(x))$
- 5: **else**
- 6: $T(x) = x - \nabla f(x)$
- 7: **end if**
- 8: {Assign dual OT losses and expectile regularisation R_g }
- 9: $L_g = -\frac{1}{n} \sum_{i=1}^n g(y_i) - \frac{1}{n} \sum_{i=1}^n g(T(x_i))$
- 10: $L_f = \frac{1}{n} \sum_{i=1}^n [c(x_i, T(x_i)) - g(T(x_i))]$
- 11: $R_g = \frac{1}{n} \sum_{i=1}^n \mathcal{L}_\tau(c(x_i, T(x_i)) - c(x_i, y_i) + g(y_i) - g(T(x_i)))$
- 12: {Apply gradient updates for parameters of models f and g }
- 13: `opt_f.minimize`(f , `loss` = L_f)
- 14: `opt_g.minimize`(g , `loss` = $L_g + \lambda R_g$)

end function

- 15: {Main train loop}
- 16: **for** $t \in 1, \dots, N$ **do**
- 17: sample $x_1, \dots, x_n \sim \alpha$, $y_1, \dots, y_n \sim \beta$
- 18: **if** `is_bidirectional` is **false** **or** $t \bmod 2 = 0$ **then**
- 19: `train_step`($f, g, \{x_1, \dots, x_n\}, \{y_1, \dots, y_n\}$)
- 20: **else**
- 21: {Update inverse mapping $\beta \rightarrow \alpha$ by swapping f and g }
- 22: `train_step`($g, f, \{y_1, \dots, y_n\}, \{x_1, \dots, x_n\}$)
- 23: **end if**
- 24: **end for**
- 25: sample $x_1, \dots, x_n \sim \alpha$, $y_1, \dots, y_n \sim \beta$
- 26: {Approximate OT distance by sum of conjugate potentials, get T from steps 2-7}
- 27: $\text{dist} = \frac{1}{n} \sum_{i=1}^n [g(y_i) + c(x_i, T(x_i)) - g(T(x_i))]$
- 28: **return** f, g, dist

5. Experiments

5.1. Results on Wasserstein-2 Benchmark

In this Section, we provide empirical evaluation of ENOT with the wall-clock time measurements on the Wasserstein-2 benchmark [Korotin et al. \(2021\)](#) and compare the results to the baseline solvers. The tasks in the benchmark consist of finding the optimal map under squared Euclidean norm $c(x, y) = \|x - y\|^2$ between either: 1) high-dimensional (HD) pairs (α, β) of Gaussian mixtures, where target measure constructed as average of gradients of learned ICNN models via [W2]

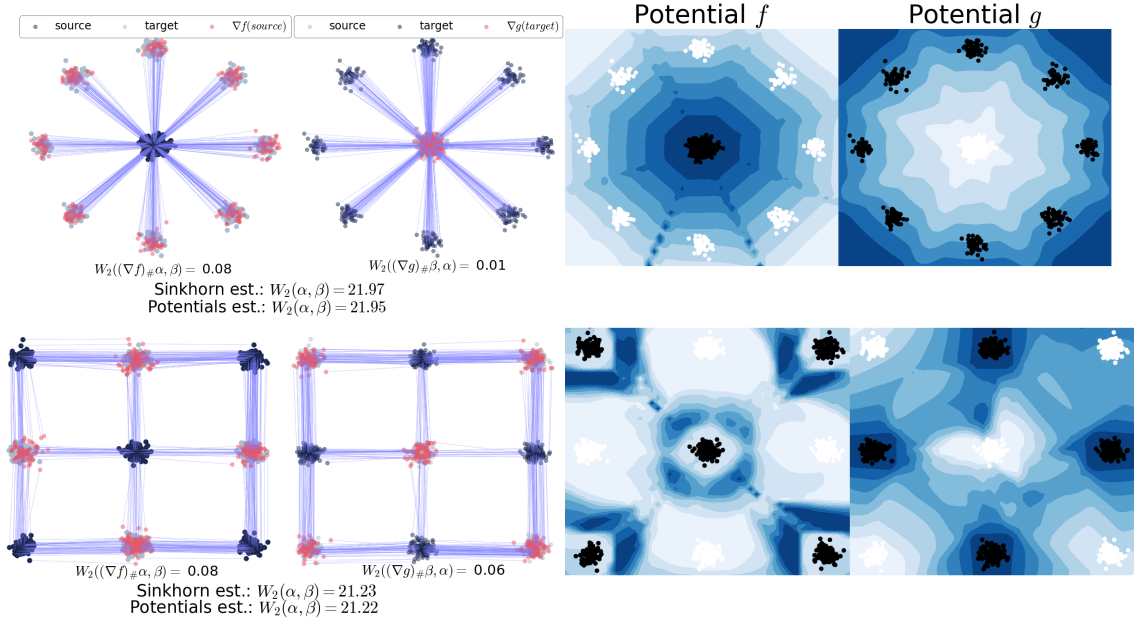


Figure 2: Recovered optimal transport plans ($\hat{T}(x)$ and $\hat{T}^{-1}(y)$ from (20)) and learned potentials contour plots obtained from solving OT dual problem (19) with squared Euclidean cost via ENOT regularisation on synthetic datasets from Makkuva et al. (2020). Evaluation metric is Sinkhorn distance between the measures, i.e. $W_2(\hat{T}_\# \alpha, \beta)$, $W_2(\alpha, \hat{T}_\#^{-1} \beta)$. The estimated distance (19) from learned potentials compared with the reference value $W_2(\alpha, \beta)$.



Figure 3: Recovered optimal transport push forward map (20) visualization for squared Euclidean cost using ENOT algorithm on synthetic datasets from Rout et al. (2021).

Korotin et al. (2019) or 2) samples from pretrained generative model W2GN (Korotin et al. (2021)) on CelebA dataset (Liu et al. (2015)). The quality of the map \hat{T} from α to β is evaluated against the ground truth optimal transport plan T^* via *unexplained variance percentage* metric ($\mathcal{L}_2^{\text{UV}}$) Korotin et al. (2019, 2021); Makkuva et al. (2020), which quantifies deviation from optimal alignment T^* , normalized by the variance of β :

$$\mathcal{L}_2^{\text{UV}}(\hat{T}, \alpha, \beta) := 100 \cdot \frac{\mathbb{E}_\alpha \|\hat{T}(x) - T^*(x)\|^2}{\text{Var}_\beta[y]} \quad (28)$$

Value of $\mathcal{L}_2^{\text{UV}}(\widehat{T}, \alpha, \beta) \approx 0$ means that \widehat{T} approximates optimal plan T^* precisely, for example in case when $\widehat{T} = \mathbb{E}[y|x]$, while values of $\mathcal{L}_2^{\text{UV}}(\widehat{T}; \alpha; \beta) \geq 100$ mean that \widehat{T} is not capable optimally reconstruct T^* . The results of the experiments are provided in Table 1 for CelebA64 and in Table 2 for the mixture of Gaussian distributions with a varying number of dimensions D . Overall, ENOT manages to approximate optimal plan T^* accurately and without any computational overhead compared to baseline methods, which require solving inner conjugate optimization loop. To be consistent with the baseline approaches, we averaged our results across 3-5 different seeds. All the hyperparameters are listed in Appendix A.2 (Table 7).

Method	Conjugate	Early Generator	Mid Generator	Late Generator
W2-Cycle	None	1.7	0.5	0.25
MM-Objective	None	2.2	0.9	0.53
MM-R-Objective	None	1.4	0.4	0.22
W2OT-Cycle	None	> 100	26.50± 60.14	0.29 ± 0.59
W2OT-Objective	None	> 100	0.29± 0.15	0.69 ± 0.9
W2OT-Cycle	L-BFGS	0.62 ± 0.01	0.20 ± 0.00	0.09 ± 0.00
W2OT-Objective	L-BFGS	0.61 ± 0.01	0.20 ± 0.00	0.09 ± 0.00
W2OT-Regression	L-BFGS	0.62 ± 0.01	0.20 ± 0.00	0.09 ± 0.00
W2OT-Cycle	Adam	0.65 ± 0.02	0.21 ± 0.00	0.11 ± 0.05
W2OT-Objective	Adam	0.65 ± 0.02	0.21 ± 0.00	0.11 ± 0.05
W2OT-Regression	Adam	0.66 ± 0.01	0.21 ± 0.00	0.12 ± 0.00
ENOT (Ours)	None	0.32 ± 0.011	0.08 ± 0.004	0.04 ± 0.002

Table 1: $\mathcal{L}_2^{\text{UV}}$ comparison of ENOT on CelebA64 tasks from the Wasserstein-2 benchmark. Attributes after method names (Cycle, Objective, Regression) correspond to the type of amortisation loss. Column Conjugate indicates the selected optimizer for the internal fine-tuning of c -conjugate transform. The results of our method include the mean and the standard deviation across 3 different seeds. The best scores are highlighted.

5.2. Results on Synthetic 2D Datasets

Additionally, we evaluate the performance of ENOT on synthetic datasets, introduced in Makuva et al. (2020) and Rout et al. (2021). Here, all neural networks are initialized as non-convex MLPs, and for each optimal plan found by ENOT, we demonstrate difference between ground truth Sinkhorn $W_2(\alpha, \beta)$ distance and optimal plan found by ENOT, which is recovered from learned potentials by equation (20). Figures 2 and 3 show the estimated optimal transport plans (in blue) both in forward and backward directions recovered by $T_{\theta\#}\alpha \approx \beta$ and $T_{\eta\#}^{-1}\beta \approx \alpha$ and the contour plots of the learned potential functions respectively. Also, in Table 4 we compare the runtime to complete 20k iterations using finetuning method from W2OT Amos (2022a) of varying number of hidden layers for non convex MLP, while keeping other hyperparameters for amortized model to those recommended from original paper with LBFGS solver. Additional details on the full list of hyperparameters is included in Appendix A.2 (Table 5).

Method	Conjugate	$D = 2$	$D = 4$	$D = 8$	$D = 16$	$D = 32$
W2-Cycle	None	0.1	0.7	2.6	3.3	6.0
MM-Objective	None	0.2	1.0	1.8	1.4	6.9
MM-R-Objective	None	0.1	0.68	2.2	3.1	5.3
W2OT-Cycle	None	0.05 ± 0.0	0.35 ± 0.01	> 100	> 100	> 100
W2OT-Objective	None	> 100	> 100	> 100	> 100	> 100
W2OT-Cycle	L-BFGS	> 100	> 100	> 100	> 100	> 100
W2OT-Objective	L-BFGS	0.03 ± 0.0	0.22 ± 0.01	0.6 ± 0.03	0.8 ± 0.11	2.09 ± 0.31
W2OT-Regression	L-BFGS	0.03 ± 0.0	0.22 ± 0.01	0.61 ± 0.04	0.77 ± 0.1	1.97 ± 0.38
W2OT-Cycle	Adam	0.18 ± 0.03	0.69 ± 0.56	1.62 ± 2.82	> 100	> 100
W2OT-Objective	Adam	0.06 ± 0.01	0.26 ± 0.02	0.63 ± 0.07	0.81 ± 0.10	1.99 ± 0.32
W2OT-Regression	Adam	0.22 ± 0.01	0.28 ± 0.02	0.61 ± 0.07	0.8 ± 0.10	2.07 ± 0.38
ENOT (Ours)	None	0.01 ± 0.0	0.03 ± 0.001	0.14 ± 0.01	0.24 ± 0.03	0.67 ± 0.02

Method	Conjugate	$D = 64$	$D = 128$	$D = 256$
W2-Cycle	None	7.2	2.0	2.7
MM-Objective	None	8.1	2.2	2.6
MM-R-Objective	None	10.1	3.2	2.7
W2OT-Cycle	None	> 100	> 100	> 100
W2OT-Objective	None	> 100	> 100	> 100
W2OT-Cycle	L-BFGS	> 100	> 100	> 100
W2OT-Objective	L-BFGS	2.08 ± 0.40	0.67 ± 0.05	0.59 ± 0.04
W2OT-Regression	L-BFGS	2.08 ± 0.39	0.67 ± 0.05	0.65 ± 0.07
W2OT-Cycle	Adam	> 100	> 100	> 100
W2OT-Objective	Adam	2.21 ± 0.32	0.77 ± 0.05	0.66 ± 0.07
W2OT-Regression	Adam	2.37 ± 0.46	0.77 ± 0.06	0.75 ± 0.09
ENOT (Ours)	None	0.56 ± 0.03	0.3 ± 0.01	0.51 ± 0.02

Table 2: $\mathcal{L}_2^{\text{UV}}$ comparison of ENOT with baseline methods on the high-dimensional (HD) tasks from Wasserstein-2 benchmark. Attributes after method names (Cycle, Objective, Regression) correspond to the type of amortisation loss. Column Conjugate indicates the selected optimizer for the internal fine-tuning of c -conjugate transform. D is the dimension of measures domain. Includes the mean and standard deviation of our method across 5 different seeds. The best scores are highlighted.

5.3. Results for Different Costs

We further investigate how ENOT performs for different instantiations of cost functions. Figures 4 and Figures 5 compare Monge gap regularization [Uscidda and Cuturi \(2023\)](#) and ENOT between measures defined on 2D synthetic datasets. We observe that despite Monge gap and ENOT recover similar transport maps T_θ , ENOT still achieves convergence up to $2\times$ faster and produces more desirable OT-like optimal maps. In order to test other specific use cases, we conducted experiments on 2-spheres dataset, where we parametrize map T_θ as MLP and tested algorithms with geodesic cost $c(x, y) = \arccos(x^T y)$ with $n = 1000$ iterations. We observed that time required for convergence is minimal for ENOT, while Monge gap requires up to $\times 3$ more time. Moreover, in our experiments

Method	$D = 2$	$D = 4$	$D = 8$	$D = 16$	$D = 32$	$D = 64$	$D = 128$	$D = 256$
W2OT	157	108	91	140	246	397	571	1028
ENOT (Ours)	14	14	15	15	15	16	21	21

Table 3: Comparison of runtimes (in minutes) against the baseline (W2OT-Objective L-BFGS) on the high-dimensional (HD) tasks from the Wasserstein-2 benchmark with same number of layers.

MLP Hidden layers	Method	Runtime
[64, 64, 64, 64]	W2OT (L-BFGS)	~ 60 min
	ENOT	~ 1.3 min
[128, 128, 128, 128]	W2OT (L-BFGS)	~ 120 min
	ENOT	~ 1.3 min
[256, 256, 256, 256]	W2OT (L-BFGS)	~ 300 min
	ENOT	~ 1.3 min

Table 4: Runtime comparison for different layers sizes between W2OT Amos (2022a) with default hyperparameters and ENOT on synthetic 2D data on tasks from Rout et al. (2021).

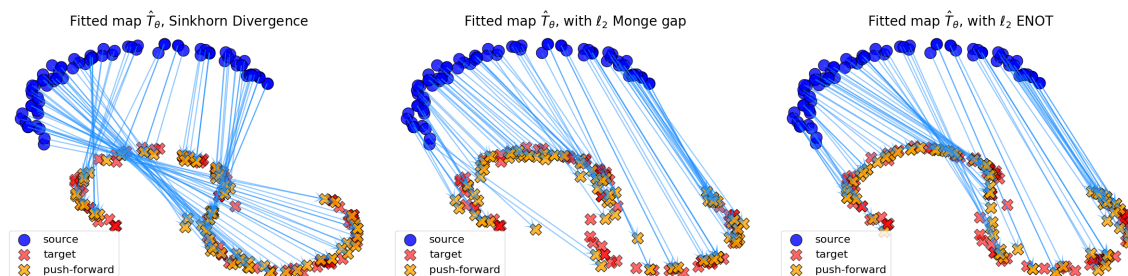


Figure 4: Fitting of three different forward transport maps T_θ between source and target measures in dimension $d = 2$ with Euclidean (not squared) cost function $c(x, y) = \|x - y\|$. We use the same number of iterations and MLP architecture for each method. **Left:** Sinkhorn divergence; **Middle:** Monge gap regularization; **Right:** ENOT regularization.

Monge gap solver diverged for $n > 1300$ iterations. Despite not having any explicit assumption on desirable map T defined in its optimization problem, ENOT estimates accurate and continuous c -OT maps.

5.4. Ablation Study on Varying Expectile τ and λ

In Figure 6, we report the study of the influence of the proposed expectile regularization on $\mathcal{L}_2^{\text{UV}}$ metric by varying the values of the expectile hyperparameter τ and the expectile loss coefficient scaling λ in Algorithm 1. Colored contour plots show areas of lowest and highest values of $\mathcal{L}_2^{\text{UV}}$. Grey areas depict cases when OT solver diverged. For example, in high-dimensions $D \geq 64$ it is the case for $\lambda = 0$, pointing out that expectile regularization parameter τ is necessary to prevent

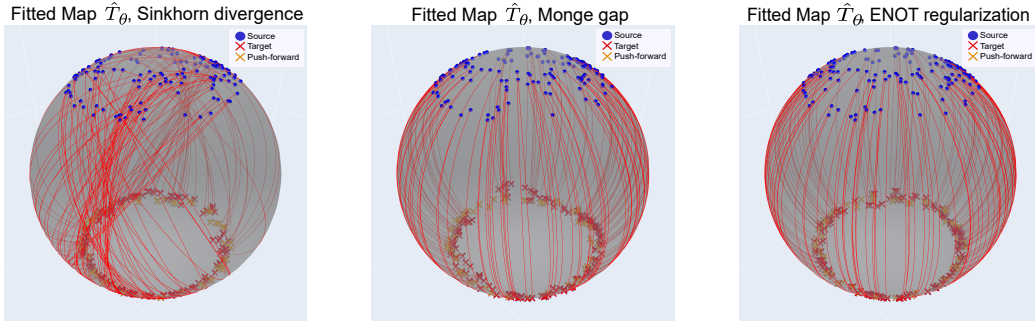


Figure 5: Recovered OT maps T_θ between synthetic measures on 2-sphere with geodesic cost $c(x, y) = \arccos(x^T y)$. All models are MLP with outputs being normalized to be on a unit sphere. **Left** : Sinkhorn divergence; **Middle**: Monge gap regularization; **Right**: ENOT regularization.

instability during training. Moreover, those figures show that despite not all choices of parameters τ and λ are being optimal, they still outperform current baseline solvers from Table 2 making whole ENOT procedure robust to extensive hyperparameter tuning on Wasserstein-2 benchmark compared to amortized optimization approach Amos (2022a), which is very sensitive to the hyperparameters of conjugate solver. All ablation study experiments were conducted using network structure and learning rates from A.2 (Table 5) (which are the same as in Table 2).

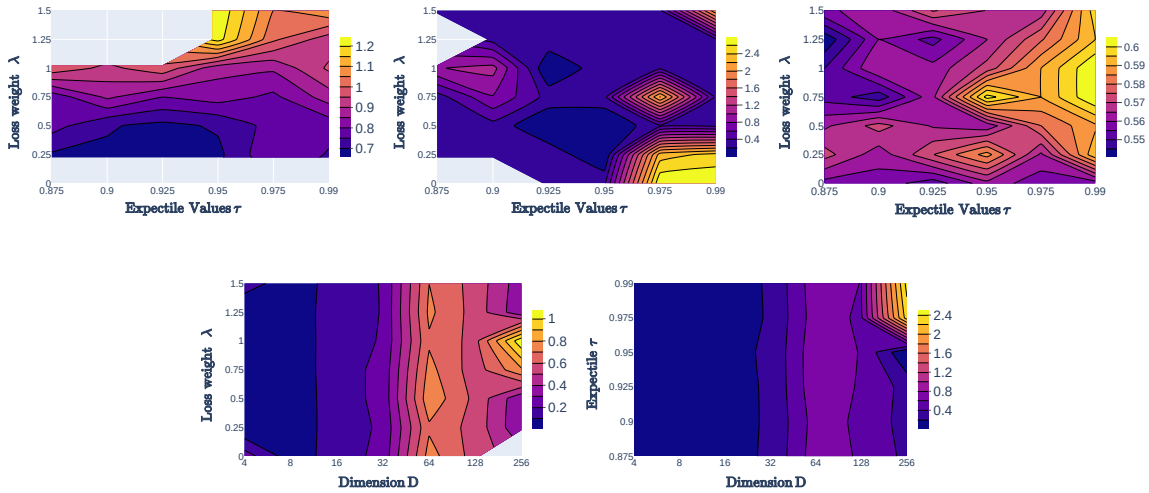


Figure 6: **Top**: Contour plots of $\mathcal{L}_2^{\text{UV}}$, depending on the values of λ and τ in Algorithm 1 for the dimensions of $D = 256$ (Left, NaN values are greyed out), $D = 128$ (Middle), and $D = 64$ (Right). **Bottom Left**: Contour plot of $\mathcal{L}_2^{\text{UV}}$, depending on the dimension D and λ coefficient with fixed expectile $\tau = 0.9$. **Bottom Right**: Contour plot of $\mathcal{L}_2^{\text{UV}}$, depending on the dimension D and expectile τ with fixed coefficient $\lambda = 0.25$.

6. Conclusion, Limitations and Future Work

Our paper introduces a new method, ENOT, for efficient computation of the conjugate potentials in neural optimal transport with the help of expectile regularisation. We formally prove that a solution to such a regularization objective is indeed a close approximation to the true c -conjugate potential. Remarkably, ENOT surpasses the current state-of-the-art approaches, yielding an up to a 10-fold improvement in terms of the computation speed on Wasserstein-2 benchmark and synthetic 2D tasks from the literature.

Despite being fast and efficient, our algorithm provides a non-exact estimation of the conjugate operator. However, we found that ENOT still outperforms the exact methods, in all our extensive tests. The proposed regularized objective on the conjugate potentials relies on two additional hyperparameters, namely: expectile coefficient τ and expectile loss tradeoff scaler λ , thus requiring a re-evaluation for new data. However, given the outcome of our ablation studies, the optimal parameters found on the Wasserstein-2 benchmark are *optimal enough* or at least provide a good starting point.

We believe that ENOT will become a new baseline to compare against for the future NOT solvers and will accelerate research in the applications of optimal transport in high-dimensional tasks, such as generative modelling. As for future directions, ENOT can be tested with the other types of cost functions, such as Lagrangian costs, defined on non-Euclidean spaces and in the dynamical optimal transport settings, such as flow matching.

References

- Luigi Ambrosio, Klaus Deckelnick, Gerhard Dziuk, Masayasu Mimura, Vsevolod A Solonnikov, Halil Mete Soner, and Luigi Ambrosio. *Lecture notes on optimal transport problems*. Springer, 2003.
- Brandon Amos. On amortizing convex conjugates for optimal transport. *arXiv preprint arXiv:2210.12153*, 2022a.
- Brandon Amos. Tutorial on amortized optimization for learning to optimize over continuous domains. *arXiv e-prints*, pages arXiv–2202, 2022b.
- Brandon Amos, Lei Xu, and J. Zico Kolter. Input convex neural networks, 2016.
- Martin Arjovsky, Soumith Chintala, and Léon Bottou. Wasserstein generative adversarial networks. In *International conference on machine learning*, pages 214–223. PMLR, 2017.
- Fabio Bellini, Bernhard Klar, Alfred Müller, and Emanuela Rosazza Gianin. Generalized quantiles as risk measures. *Insurance: Mathematics and Economics*, 54(C):41–48, 2014.
- Iaroslav Bespalov, Nazar Buzun, and Dmitry V Dylov. Brulé: Barycenter-regularized unsupervised landmark extraction. *Pattern Recognition*, 131:108816, 2022a.
- Iaroslav Bespalov, Nazar Buzun, Oleg Kachan, and Dmitry V Dylov. Lambo: Landmarks augmentation with manifold-barycentric oversampling. *IEEE Access*, 10:117757–117769, 2022b.
- Lukas Biewald. Experiment tracking with weights and biases, 2020. URL <https://www.wandb.com/>. Software available from wandb.com.

- James Bradbury, Roy Frostig, Peter Hawkins, Matthew James Johnson, Chris Leary, Dougal Maclaurin, George Necula, Adam Paszke, Jake VanderPlas, Skye Wanderman-Milne, and Qiao Zhang. JAX: composable transformations of Python+NumPy programs, 2018. URL <http://github.com/google/jax>.
- Yann Brenier. Polar factorization and monotone rearrangement of vector-valued functions. *Communications on pure and applied mathematics*, 44(4):375–417, 1991.
- Charlotte Bunne, Laetitia Papaxanthos, Andreas Krause, and Marco Cuturi. Proximal optimal transport modeling of population dynamics. In *International Conference on Artificial Intelligence and Statistics*, pages 6511–6528. PMLR, 2022.
- Nazar Buzun. Gaussian Approximation for Penalized Wasserstein Barycenters. *Math. Meth. Stat.*, 32(3):1–26, 2023. doi: 10.3103/S1066530723010039. URL <https://doi.org/10.3103/S1066530723010039>.
- Yucheng Chen, Matus Telgarsky, Chao Zhang, Bolton Bailey, Daniel Hsu, and Jian Peng. A gradual, semi-discrete approach to generative network training via explicit wasserstein minimization, 2019.
- Djork-Arné Clevert, Thomas Unterthiner, and Sepp Hochreiter. Fast and accurate deep network learning by exponential linear units (elus), 2015.
- Marco Cuturi. Sinkhorn distances: Lightspeed computation of optimal transport. *Advances in neural information processing systems*, 26, 2013.
- Marco Cuturi, Laetitia Meng-Papaxanthos, Yingtao Tian, Charlotte Bunne, Geoff Davis, and Olivier Teboul. Optimal transport tools (ott): A jax toolbox for all things wasserstein. *arXiv preprint arXiv:2201.12324*, 2022.
- Nhan Dam, Quan Hoang, Trung Le, Tu Dinh Nguyen, Hung Bui, and Dinh Phung. Three-player wasserstein gan via amortised duality. In *Proceedings of the Twenty-Eighth International Joint Conference on Artificial Intelligence, IJCAI-19*, pages 2202–2208. International Joint Conferences on Artificial Intelligence Organization, 7 2019. doi: 10.24963/ijcai.2019/305. URL <https://doi.org/10.24963/ijcai.2019/305>.
- John M Danskin. The theory of max-min, with applications. *SIAM Journal on Applied Mathematics*, 14(4):641–664, 1966.
- Jiaojiao Fan, Amirhossein Taghvaei, and Yongxin Chen. Scalable computations of wasserstein barycenter via input convex neural networks, 2020.
- Arnaud Fickinger, Samuel Cohen, Stuart Russell, and Brandon Amos. Cross-domain imitation learning via optimal transport. *arXiv preprint arXiv:2110.03684*, 2021.
- Ishaan Gulrajani, Faruk Ahmed, Martin Arjovsky, Vincent Dumoulin, and Aaron C Courville. Improved training of wasserstein gans. *Advances in neural information processing systems*, 30, 2017.

- Siddhant Haldar, Vaibhav Mathur, Denis Yarats, and Lerrel Pinto. Watch and match: Supercharging imitation with regularized optimal transport. In *Conference on Robot Learning*, pages 32–43. PMLR, 2023.
- Diederik P. Kingma and Jimmy Ba. Adam: A method for stochastic optimization, 2014.
- Alexander Korotin, Vage Egiazarian, Arip Asadulaev, Alexander Safin, and Evgeny Burnaev. Wasserstein-2 generative networks. *arXiv preprint arXiv:1909.13082*, 2019.
- Alexander Korotin, Lingxiao Li, Aude Genevay, Justin M Solomon, Alexander Filippov, and Evgeny Burnaev. Do neural optimal transport solvers work? a continuous wasserstein-2 benchmark. *Advances in Neural Information Processing Systems*, 34, 2021.
- Alexander Korotin, Daniil Selikhanovych, and Evgeny Burnaev. Neural optimal transport. *arXiv preprint arXiv:2201.12220*, 2022.
- Alexey Kroshnin, Vladimir Spokoiny, and Alexandra Suvorikova. Statistical inference for Bures–Wasserstein barycenters. *The Annals of Applied Probability*, 31(3):1264 – 1298, 2021. doi: 10.1214/20-AAP1618. URL <https://doi.org/10.1214/20-AAP1618>.
- Jacob Leygonie, Jennifer She, Amjad Almahairi, Sai Rajeswar, and Aaron Courville. Adversarial computation of optimal transport maps. *arXiv preprint arXiv:1906.09691*, 2019.
- Huidong Liu, Xianfeng Gu, and Dimitris Samaras. Wasserstein gan with quadratic transport cost. In *Proceedings of the IEEE/CVF International Conference on Computer Vision (ICCV)*, October 2019a.
- Huidong Liu, Xianfeng Gu, and Dimitris Samaras. Wasserstein gan with quadratic transport cost. In *Proceedings of the IEEE/CVF international conference on computer vision*, pages 4832–4841, 2019b.
- Ziwei Liu, Ping Luo, Xiaogang Wang, and Xiaoou Tang. Deep learning face attributes in the wild. In *Proceedings of the IEEE international conference on computer vision*, pages 3730–3738, 2015.
- Yicheng Luo, Zhengyao Jiang, Samuel Cohen, Edward Grefenstette, and Marc Peter Deisenroth. Optimal transport for offline imitation learning. *arXiv preprint arXiv:2303.13971*, 2023.
- Ashok Makkuva, Amirhossein Taghvaei, Sewoong Oh, and Jason Lee. Optimal transport mapping via input convex neural networks. In *International Conference on Machine Learning*, pages 6672–6681. PMLR, 2020.
- Anton Mallasto, Jes Frellsen, Wouter Boomsma, and Aasa Feragen. (q,p)-wasserstein gans: Comparing ground metrics for wasserstein gans, 2019.
- Eduardo Fernandes Montesuma, Fred Ngolè Mboula, and Antoine Souloumiac. Recent advances in optimal transport for machine learning, 2023.
- Whitney Newey and James Powell. Asymmetric least squares estimation and testing. *Econometrica*, 55(4):819–47, 1987.

- Georgios Papagiannis and Yunpeng Li. Imitation learning with sinkhorn distances. In *Joint European Conference on Machine Learning and Knowledge Discovery in Databases*, pages 116–131. Springer, 2022.
- Gabriel Peyré, Marco Cuturi, et al. Computational optimal transport: With applications to data science. *Foundations and Trends® in Machine Learning*, 11(5-6):355–607, 2019.
- Litu Rout, Alexander Korotin, and Evgeny Burnaev. Generative modeling with optimal transport maps, 2021.
- Filippo Santambrogio. Optimal transport for applied mathematicians. *Birkäuser, NY*, 55(58-63):94, 2015.
- Jian Shen, Yanru Qu, Weinan Zhang, and Yong Yu. Wasserstein distance guided representation learning for domain adaptation. In *Proceedings of the AAAI Conference on Artificial Intelligence*, volume 32, 2018.
- Nikolay Shvetsov, Nazar Buzun, and Dmitry V. Dylov. Unsupervised non-parametric change point detection in electrocardiography. *Proceedings of the 32nd International Conference on Scientific and Statistical Database Management*, 2020. URL <https://api.semanticscholar.org/CorpusID:220872006>.
- Amirhossein Taghvaei and Amin Jalali. 2-wasserstein approximation via restricted convex potentials with application to improved training for gans, 2019.
- Théo Uscidda and Marco Cuturi. The monge gap: A regularizer to learn all transport maps. *arXiv preprint arXiv:2302.04953*, 2023.
- Cédric Villani et al. *Optimal transport: old and new*, volume 338. Springer, 2009.
- Yujia Xie, Minshuo Chen, Haoming Jiang, Tuo Zhao, and Hongyuan Zha. On scalable and efficient computation of large scale optimal transport. In *International Conference on Machine Learning*, pages 6882–6892. PMLR, 2019.
- Omry Yadan. Hydra - a framework for elegantly configuring complex applications. Github, 2019. URL <https://github.com/facebookresearch/hydra>.

Appendix A. Implementation Details

A.1. Environment

We implement ENOT in JAX framework [Bradbury et al. \(2018\)](#), making it fully compatible and easily integrable with the OTT-JAX library [Cuturi et al. \(2022\)](#). Moreover, since ENOT introduced expectile regularization, there is no additional overhead and whole procedure is easily *jit*-compiled. To find the optimal hyperparameters in [Appendix A.2](#), we used Weights & Biases [Biewald \(2020\)](#) sweeps for hyperparameter grid search and Hydra [Yadan \(2019\)](#) for managing different setup configurations. ENOT implementation consists of only a single file, which is easy to reproduce and can be tested on other datasets of interest.

A.2. Hyperparameters for Wasserstein-2 Benchmark Tasks

Tables 5 and 7 provide detailed hyperparameter values used in the experiments in Section 5. To find the values of these parameters, we performed an extensive grid search sweep across different seeds, yielding the best results among the seeds, on average. We tried to be as close as possible in terms of hyperparameters to previous works. Likewise, we tested different choices of hidden layers and found that the most stable training occurs at $n \geq 512$, but we found that for low-dimensional tasks (i.e $D \leq 64$), 128 neurons are enough to achieve lowest \mathcal{L}^2 -UVP compared to results reported in Amos (2022a); Makuva et al. (2020); Korotin et al. (2022). Since ENOT does not introduce any additional computational overhead, increasing number of neurons will not slow down overall training time. Runtime comparison with Amos (2022a) for W-2 benchmark presented in Table ??.

Hyperparameter	Value
potential model f_θ	non-convex MLP
conjugate model g_θ	non-convex MLP
f_θ hidden layers	[512, 512, 512] if $D \geq 64$, else [128, 128, 128]
g_θ hidden layers	
# training iterations	200 000
activation function	ELU Clevert et al. (2015)
f optimizer	Adam Kingma and Ba (2014) with cosine annealing ($\alpha = 1e-4$)
g optimizer	
Adam f β	[0.9, 0.9]
Adam g β	[0.9, 0.7]
initial learning rate	3e-4
expectile coef. λ	0.3
expectile τ	0.9
batch size	1024

Table 5: Hyperparameters for D -dimensional Gaussian Mixture Wasserstein-2 benchmark tasks.

Hyperparameter	Value
potential model f_θ	non-convex MLP
conjugate model g_θ	non-convex MLP
f_θ hidden layers	[64, 64, 64, 64]
g_θ hidden layers	
# training iterations	100 000
activation function	ELU Clevert et al. (2015)
f optimizer	Adam Kingma and Ba (2014) with cosine annealing ($\alpha = 1e-4$)
g optimizer	
Adam f β	[0.9, 0.999]
Adam g β	
initial learning rate	5e-4
expectile coef. λ	0.3
expectile τ	0.99
batch size	10 000

Table 6: Hyperparameters for Synthetic 2D datasets from Rout et al. (2021)

Hyperparameter	Value
potential model f_θ	ConvPotential Amos (2022a)
conjugate model g_θ	
hidden layers	6 Conv Layers
# training iterations	80 000
activation function	ELU Clevert et al. (2015)
f optimizer	Adam Kingma and Ba (2014) with cosine annealing ($\alpha = 1e-4$)
g optimizer	
Adam f β	
Adam g β	[0.5, 0.5]
initial learning rate	3e-4
expectile coef. λ	1.0
expectile τ	0.99
batch size	64

Table 7: Hyperparameters for CelebA64 Wasserstein-2 benchmark tasks.

A.3. Synthetic 2D Tasks Details

Table 6 lists optimal parameters for ENOT for synthetic-2D tasks from Rout et al. (2021). Amos (2022a) pointed out that LeakyReLU activation works better compared to ELU used for Wasserstein-2 benchmark. However, for expectile regularisation we found out that ELU works as well for synthetic 2d tasks. We keep Adam β parameters as default [0.9, 0.999] and observe that 25k training iterations are enough to converge for tasks from Rout et al. (2021). Moreover, we tried different neurons per layer and Table 4 shows runtime in minutes in comparison to previous state-of-the-art approach. Such speedups are made possible due to efficient utilization of `jit` compilation since ENOT does not use any inner optimizations.

A.4. W2-Benchmark Tasks Details

High-dimensional measures (HD) task from Korotin et al. (2019) tests whether OT solvers can redistribute mass among modes of varying measures. Different instantiations of Gaussian mixtures in dimensions $D=2, 4, 16, \dots, 256$ are compared between each other via OT. In the benchmark, `Mix3toMix10` is used, where source measure α can consist of random mixture of 3 Gaussians and target measure consist of two random mixtures β_1, β_2 of 10 Gaussians. Afterwards, pretrained OT potentials $\nabla\psi_i \# \alpha = \beta$ are used to form the final pair as $(\alpha, \frac{1}{2}(\nabla\psi_1 + \nabla\psi_2) \# \alpha)$. Figure 7 visualizes such pair of measures.

Images task produces pair candidates for OT solvers in the form of high-dimensional images from CelebA64 faces dataset Liu et al. (2015). Different pretrained checkpoints (Early, Mid, Late, Final) from WGAN-QC model Liu et al. (2019a) are used to pretrain potential models. Target measure for final checkpoint is constructed as average between learned potentials via [W2] solver and forms a pair input for OT algorithm as $(\alpha_{\text{CelebA}}, \beta_{\text{ckpt}}) = (\alpha_{\text{Final}}, \frac{1}{2}(\nabla\psi^1 + \nabla\psi^2) \# \alpha_{\text{Final}})$. Figure 8 shows an example of pair of two such measures (α, β) .

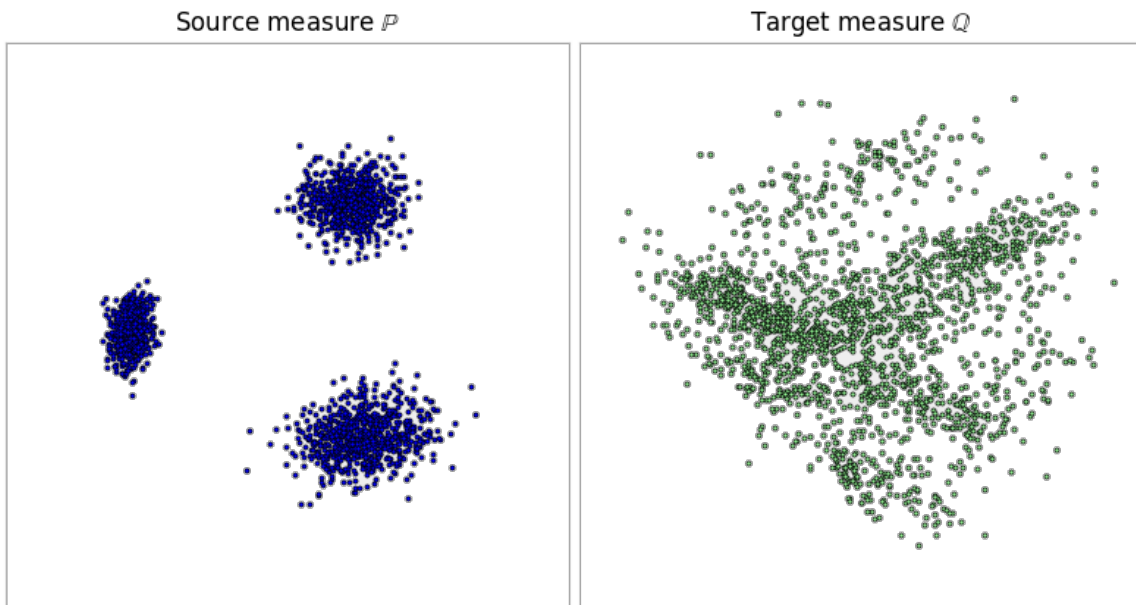


Figure 7: Sample example of pair of measures from $Mix3toMix10$

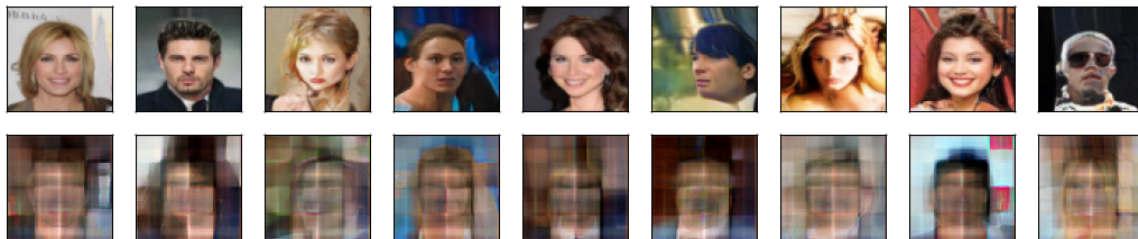


Figure 8: Example pair from W2-Benchmark of CelebA faces. **Top row:** Images, which were produced as final checkpoint from WGAN-QC model. **Bottom row:** Images, obtained from early checkpoint of WGAC-QC model.

A.5. Additional Results on W2-Benchmark CelebA64

Figure 9 shows ENOT training metrics on CelebA64 early checkpoint for 80k training iterations with parameters listed in Table 7. On this figure, we report metrics from Korotin et al. (2019). Namely: W^2 distance between initial source and predicted source samples under map $T(x) = \nabla_x f(x)$ and cosine similarity metrics, which measures *alignment* between plans. We refer reader to original paper Korotin et al. (2019), where additional details on metrics evaluation as well as other baseline metrics such as identity, constant and linear are introduced.

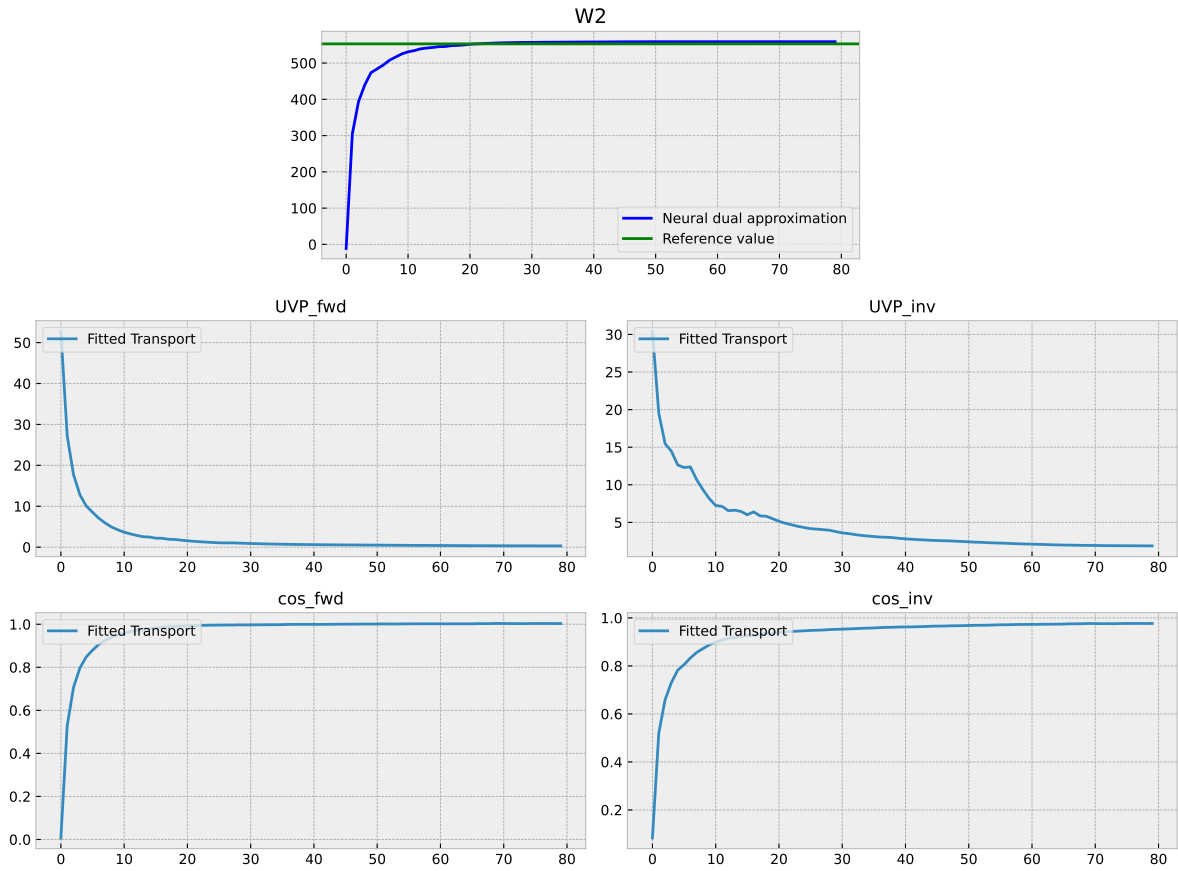


Figure 9: ENOT training metrics from on W2-benchmark on CelebA64 Early task.